ULTRASTRUCTURE AND RELEASE CHARACTERISTICS OF HYPER-COMPLIANT MICROPARTICLES FOR HYDROPHOBIC DRUG DELIVERY

By

Rebeka Sowers

B.S. Biological Sciences, California Polytechnic State University, 2021

Thesis

Submitted in partial fulfillment of the requirements for the Degree of Master of Science in the Graduate Program of Biotechnology at Brown University

PROVIDENCE, RHODE ISLAND

MAY 2023

AUTHORIZATION TO LEND AND REPRODUCE THE THESIS

As the sole author of this thesis, I authorize Brown University to lend it to other institutions for the purpose of scholarly research.

Date 05/01/2023 Rebeka Sowers

Rebeka Sowers, Author

I further authorize Brown University to reproduce this thesis by photocopying or other means, in total or in part, at the request of other institutions or individuals for the purpose of scholarly research.

Date 05/01/2023 Rebeka Sowers

Rebeka Sowers, Author

This thesis by Rebeka Sowers is accepted in its present form by the Graduate Program in Biotechnology as satisfying the thesis requirements for the degree of Master of Science

Date_____ Signature: _____

Dr. Eric M. Darling, Advisor

Date_____ Signature: _____

Dr. Edith Mathiowitz, Reader

Date_____ Signature: _____

Dr. Diana Horrigan, Reader

Approved by the Graduate Council

Date_____ Signature: _____

Dr. Thomas Lewis, Dean of the Graduate School

Acknowledgements

Firstly, I would like to thank my advisor, Dr. Eric Darling for his excellent mentorship and guidance, encouraging me to pursue my interests and always being incredibly generous with his time and feedback. The Darling Lab members should also not go unnoticed, as they have cultivated a safe space and close-knit community that made coming into lab every day so enjoyable. Thank you to Dr. Edith Mathiowitz for teaching me about the world of drug delivery and polymers, a topic I knew little about before starting this research. Thank you for also taking the time to serve on my committee, along with Dr. Diana Horrigan, providing valuable feedback that has improved this thesis. I would also like to express my gratitude towards Dr. Jacquelyn Schell for putting so much time and effort into being the program director and ensuring that I stayed on track to graduate. Lastly, I would like to thank my friends and family who have always pushed me to be the best, hardest-working, and most confident version of myself. I attribute my success to all of you, thank you.

Table of Contents

Table of Tables

Table of Figures

Abstract of Ultrastructure and Release Characteristics of Hyper-Compliant Microparticles for Hydrophobic Drug Delivery, by Rebeka Sowers, ScM., Brown University, May 2023.

The use of soft, cell-like microparticles as a carrier for drug nanocrystals holds great promise in the drug delivery field. Research shows that microparticles with similar elastic properties to mammalian cells allow them to bypass organs, leading to longer circulation times *in-vivo*. The goal of this study was to characterize and compare soft, 0.25 kPa hyper-compliant polyacrylamide microparticles to stiff, 10 kPa microparticles by analyzing the nano and ultrastructure properties giving rise to the different elasticities. We also establish feasibility for entrapping model hydrophobic drug, dexamethasone nanocrystals, and compare *in-vitro* release rates to that of free, non-entrapped drug to test the hypothesis that the microparticles will not have an effect on release. Ultrastructure of monodisperse, 12 μm particles of both soft and stiff formulations was investigated using cryo-scanning electron microscopy. To determine the effective permeability of the hydrogel polymer network, a size exclusion assay with varying sizes of FITC-dextran was performed. Confocal microscopy was used to visualize the fluorescent molecule permeation into the hyper-compliant microparticles. Release experiments used microparticles in which the water in the prepolymer solution was substituted with a sonicated suspension of dexamethasone. Aliquots from release media were taken at predetermined time points and analyzed over 96 hours for their drug concentration. Microparticles featured non-interconnected pores, with the 0.25 kPa formulation exhibiting significantly smaller pore size diameters and thinner polymer pore walls than the 10 kPa particles. Dextran size exclusion studies indicated that the soft hydrogel's maximum effective permeability was 22 nm, more than double that of the stiff hydrogel's network. This allows larger nanocrystals to be retained in the network, and only solubilized drug to diffuse out. Free dexamethasone exhibited a slightly faster dissolution than entrapped drug within the first four hours, but the overall release profile was not substantially different. These findings show that hydrophobic drugs can be entrapped in hyper-compliant microparticles without disrupting their structure or elasticity. Furthermore, because the microparticles do not hinder release, drug-entrapped nanoparticles for controlled, long-term delivery could be carried in the microparticles to avoid physiological filtration methods.

Introduction

Intravenous (IV) is one of the most common types of drug administration because it avoids the first-pass effect, which occurs when a large percentage of the drug gets metabolized before reaching systemic circulation.[1] IV is the best way to administer drugs that need to reach the bloodstream quickly and bypass the harsh conditions of the stomach. It can be given as a bolus, a quick acting administration for emergencies, or as an infusion, when continual exposure is needed to induce the therapeutic effect.[2] This requirement for recurrent exposure is one of the main disadvantages of IV administration, generating the need for a drug delivery system (DDS) to control release rates, leading to less frequent subjection to infusion and higher patient compliance.

Micro and nano encapsulation for controlled drug delivery provide solutions to the disadvantages associated with IV administration, such as protecting the encapsulated drug from degradation, permitting more control over release rates, and easier administration compared to controlled release implants.[3] Microparticles (MPs) and nanoparticles (NPs) can exist in a matrix system, in which the drug is dispersed throughout the polymer, or a reservoir system, when a distinct shell surrounds the drug-filled core.[4] Drugs can release from particles via diffusion, dissolution, osmosis, or erosion depending on the polymer's and drug's physical and chemical properties.[4] Polymers used for encapsulated drug delivery can have different shapes, sizes, surface chemistries, and deformability properties, all of which are important factors for particle circulation, margination, and appropriate interaction with immune cells.[5] Cooley et al., describes a study in which four distinct shapes, ranging from the nano to micro scale are computationally and experimentally tested by their margination in blood flow.[6] Results revealed that micro-scale particles have higher margination compared to nano-scale particles, supporting the evidence that microparticles exhibit better vascular targeting.[5, 6] Particle size also affects removal from the body

via immune cells. After systemic administration, nanoparticles are typically cleared in under an hour by a multitude of methods, such as phagocytosis, pinocytosis, and scavenger receptor-mediated endocytosis.[5,7] Microparticles similar to cell size may be able to circulate for longer, but because materials used in the drug delivery space often exhibit stiffer properties than native cells, microparticles carry a higher risk of capillary occlusion and blocking blood flow.[5, 8]

Polymeric particles have been used to deliver a variety of cargo parenterally, such as steroids, proteins, and peptides, which have great therapeutic potential, but are often limited due to unsuccessful delivery or shortened circulation times.[9] A study describing *in-vitro* sustained release of dexamethasone (DEX) from PLGA nanoparticles reveals a fast release of 60% in the first two days, and a 90% release within two weeks.[10] These nanoparticles were also embedded in hydrogel matrices, showing a more extended release, reaching only 80% in three weeks.[10] While this study successfully demonstrated *in-vitro* sustained release, elongated circulation is another pertinent property in allowing long-term delivery from particles *in-vivo*.

To increase particle circulation times for long-term release, surface modifications can be employed. Decorating surfaces with proteins or vascular-targeted ligands have the potential to localize particles and accumulate at sites of inflammation, extending presence in the body.[5] Coating particles with polyethylene glycol (PEG), also known as PEGylation is another way to increase half-life elimination.[7] This modification can shield the surface from aggregation, opsonization, and phagocytosis, and has also been shown to increase residence time through other routes of administration.[7] However, the overuse of PEG has also led to the detection of PEG-specific antibodies, decreasing its therapeutic potential in the drug delivery field.[5]

Deformability, or elasticity is another major property governing circulation time. The degree of crosslinking determines a hydrogel particle's elastic modulus and flexibility, and can be

leveraged to decrease phagocytosis and improve vascular localization and navigation.[5] A study analyzing particle elasticity examined nanoparticles ranging from 10 kPa to 3,000 kPa, with the lower end correlating to more deformable particles and longer circulation times, and vice versa.[11] Results showed that the 10 kPa nanoparticles exhibited a higher persistence in the blood and reduced cellular uptake *in-vivo.*[11] However, microparticles must have a lower elastic modulus than these nanoparticles because they run a higher risk of occlusion.

Mammalian blood cells possess elastic properties that allow them to readily pass through small capillaries, the same of which can be applied to microparticles to overcome the risk of occlusion.[8] Merkel et al. fabricated hydrogel microparticles to mimic the shape, size, and elasticity of mouse RBCs, and examined circulation times as a function of deformability.[8] The microparticles were 5.2-5.9 μm in diameter, with elastic moduli ranging from 7.8 to 63.9 kPa, while 0.11 – 4.89 kPa is the reported elastic moduli for various spots on RBCs.[8, 12] Results showed that the deformable microparticles were able to bypass organs that the stiffer particles were caught in, leading to longer circulation times.[8] Although there has been some evidence that microparticles are quickly phagocytosed in the body, this study revealed that an 8-fold decrease in elastic modulus correlated to over a 30-fold extension of the elimination half-life. The Mathiowitz and Darling Laboratories at Brown University created the first microparticles with characteristics that mimic the size, elasticity, and spherical shape of mammalian cells.[13] These hyper-compliant microparticles (HCMPs) made from polyacrylamide through inverse emulsion range from 5-40 μm and possess tunable mechanical properties from 0.25 – 10 kPa.[13]

Methods

Hyper-compliant microparticle fabrication

Cell-like HCMPs with an elastic modulus of 0.25 kPa were fabricated as an inverse bulk emulsion based on the previously described microparticles created in the Darling and Mathiowitz Laboratories at Brown University.[13] The dispersed, or aqueous phase was created in a 1.7 mL conical tube, consisting of 4% acrylamide (MilliporeSigma), 0.05% bis-acrylamide (Fisher), 0.1% initiator, ammonium persulfate (APS) (Fisher BioReagents), and 1% catalyst, TEMED (Fisher) (116 g/mol). The remaining percentage was filled with DI H_2O to equate to 400 μL total in volume. Contents were vortexed and added to 3-5x volume of the continuous (oil) phase, 1-octadecene (Sigma-Aldrich) containing 1% Hypermer 1031 (Croda) quickly after mixing in the TEMED to produce an inverse emulsion. Particles were left for 30 minutes at room temperature to ensure crosslinking. Emulsion was centrifuged at ~10,000 rcf for two seconds to separate the dispersed and continuous phase. The top layer (continuous) was removed, and particles were washed three times with 0.1% triton X-100 solution (Fisher) to remove the oil followed by three DI H_2O washes to remove any remaining triton X-100. Particles were resuspended in 1 mL DI H_2O. To fabricate a stiffer, 10 kPa version of the microparticles, acrylamide and bis-acrylamide were increased to 8% and 0.3% of the total volume, respectively. The remaining volume was filled with DI H_2O.

Ultrasound sonication treatment has been shown to be an important factor in reducing particulate size.[14] To break down large dexamethasone aggregates into small nanocrystals for entrapment, a sonication technique was used. DEX powder was suspended at ~50 mg/mL (Tokyo Chemical Industry) in DI H_2O containing 0.5% Pluronic F-127 surfactant (Thermo Fisher) to help facilitate wetting and dispersion of dexamethasone.[15] A probe sonicator (Q55, Qsonica) with a nominal power of 50 W was submerged into the suspension without touching the bottom of the

tube. During sonication, the tube was placed in a beaker of ice water and agitated for 20 minutes in 45 seconds on, 15 seconds off fashion to avoid overheating. To create DEX-entrapped HCMPs, the sonicated DEX suspension replaced the full volume of DI H_2O in the prepolymer solution. DEX nanocrystal aggregate size and HCMPs were imaged using simple polarization and brightfield microscopy with Q-capture imaging software.

The elastic properties of these control and DEX-entrapped HCMPs were investigated through previously described indentation testing using an MFP-3D-Bio atomic force microscope (AFM, Asylum Research, Santa Barbara, CA) with a spherically tipped cantilever.[13] From a DEX-entrapped HCMP batch, empty microparticles containing no DEX were tested alongside microparticles with entrapped dexamethasone. An approach velocity of 10 μm/s was applied with a trigger force of 1.5 nN, correlating to a 1-2 μm indentation. A force vs. indentation curve was created to obtain the elastic moduli of both empty and DEX-entrapped HCMPs made by bulk emulsion.

Cryo-scanning electron microscopy

Investigation of HCMP ultrastructure was performed using a Zeiss Sigma VP field emission scanning electron microscope (SEM) equipped with a cryogenic chamber and cold stage (Gatan Alto 2500) at the Rhode Island Consortium of Nanoscience and Nanotechnology at the University of Rhode Island. In session one, 0.25 and 10 kPa microparticles created via bulk emulsion were imaged, while sessions two and three imaged microparticles created via droplet generation described in Dubay, et al.[16] Prior to imaging, particles were spun down and resuspended in 0.5-1 mL DI H_2O to create a concentrated suspension. For each sample (soft and stiff), three to four droplets of the microparticle suspension were pipetted onto a cryo-SEM stub, equally spaced

apart. The stub containing the droplets was quickly submerged into a liquid nitrogen slush to avoid losing any droplets. The stub was then transferred to the prechamber under vacuum, which was cooled down to -130℃. Samples were gently fractured using a cold flat-edge knife and sublimed for three minutes at -100℃. After subliming, the sample was cooled back to -130℃. Imaging was performed in variable pressure mode (30 Pa) using the backscatter detector (EHT = 10 kV). Particles were not sputter-coated. Images were taken by first scanning the droplet to locate a field of particles. Once there was a view of interest, the microparticles were used as a focus for the microscope to zoom in on. The contrast and amount of light was adjusted to appropriately view the particles.

Analysis of cryo-SEM images was performed in ImageJ. To investigate if the sublimation preparation process changed the size of the particles, the diameter of soft and stiff particles from session two was calculated in ImageJ, assuming circular shape. Individual pore size diameter for each formulation was determined by manually tracing pores from a distribution of images from session two. Microparticles from session three were analyzed for their polymer pore wall thickness by measuring mean gray value per particle. This was done by setting a black and white threshold adjusted so that as much of the polymer was showing in white, while still maintaining a black background. A circle was then drawn around the particle, and the mean gray value was measured, with a lower limit of 0 (black) and an upper limit of 255 (white).

FITC-dextran size exclusion assay

Fluorescent isothiocyanate (FITC) is often used in permeability assays because it is easily detected with fluorescence, and varying weights of dextran molecules can be attached to measure exclusion.[17] In this study, FITC-dextran was used to indirectly estimate the effective permeability

of the 0.25 and 10 kPa empty HCMP hydrogel network. FITC-dextran (MilliporeSigma) with increasing molecular weights (MW) shown in table 1, were dissolved in 1x PBS to achieve a final concentration of 0.065 mg/mL (molarity = $1.63x10^{-6}$, $2.60x10^{-7}$, $3.25x10^{-8}$ mol/L for 40, 250, and 2000 kDa, respectively). FITC alone was used as a positive control, diluted to 0.004 mg/mL in 1x PBS. Low concentrations of FITC were required to stay within the excitation wavelength of the microscope. To decrease measurement error, a highly concentrated stock solution was first created before further diluting in 1x PBS.

FITC-dextran size (kDa)	Hydrodynamic Diameter (nm)
0 (FITC control)	0
40	9
250	22
2000	63

Table 1. *FITC-dextran sizes corresponding to reported radii (Å) were converted to hydrodynamic diameter in nanometers for better understanding of size.*[18] *Free FITC (no dextran) was used as a positive control for complete permeation into the microparticles.*

Monodispersed, droplet-generated 0.25 and 10 kPa microparticles dyed with pink rhodamine (Sharpie) were centrifuged and resuspended in the FITC-dextran and free FITC solutions. Suspensions were equilibrated overnight to ensure complete permeation of FITC-dextran molecules into the hydrogel mesh. Images were taken on an Olympus FV3000 confocal microscope using Alexa 488 (green) and Alexa 568 (red) channels to see the emitted wavelength from FITC and Sharpie die, respectively.

Image processing on 2-4 images containing anywhere from 100-400 microparticles for every treatment was performed using ImageJ and MATLAB. Image channels were split in ImageJ to reveal the individual Alexa 488 and Alexa 568 images. The contrast between the particles and

background on the red channel were used as a guide in the MATLAB script for locating the particles on the green channel, where FITC-dextran exclusion could be observed. A trim radius of 20% was employed and the mean FITC signal intensity within the particle region, μp, and the background, μo, was found. To quantify the permeation of FITC-dextran and FITC into the soft and stiff polyacrylamide microparticles, the fluorescence signal intensity ratio between the particles and background was calculated, given by μp/μo.

In-vitro dissolution studies

Dexamethasone-entrapped HCMPs were fabricated and washed as previously described, and then placed in a 50 mL DI H_2O sink. Simultaneously, free dexamethasone of matched concentration from the same sonicated suspension was placed in another DI H_2O sink. Three experimental replicate pairs were fabricated, each pair consisting of one DEX HCMP sample, and one matched free DEX sample. A sink containing empty microparticles was used as a control. After placing samples in the sink, tubes were gently inverted and allowed to settle for 10 minutes before taking the first time point. Time points were then taken at t = 30, 50, 70, 120, 180, 240 minutes, and once at 24, 48, 72, and 96 hours, inverting after each time point. Aliquots were taken in triplicate from the top half of the sink to ensure only dissolved DEX was being read. A BioTek Cytation 3 Cell Imaging Multi-Mode Reader was used to measure UV-Vis at 242 nm (λ max) in a quartz 96-well plate. [19] Images of the DEX HCMP particles were taken over the course of the experiment.

A standard curve of dexamethasone vs. absorbance was created using serial dilutions of known DEX concentrations, 88, 44, 22, 11, 5.5, 2.75, 1.375, 0.6875 μg/mL. A stock solution of 4.4 mg DEX was dissolved in 50 mL (0.088 mg/mL) of DI H_2O (solubility limit = 0.1 mg/mL).[19]

This solution was then serially diluted by a factor of two in DI H_2O to produce the desired concentrations. Absorbance was measured using UV-Vis on the BioTek Cytation and plotted against concentration. The standard curve equation was used to calculate the unknown concentration of DEX in the sink at each time point. Values were then normalized against the maximum concentration dissolved for each respective DEX HCMP and free DEX replicate and multiplied by 100. Dissolution profiles of all samples were fit to the Ritger Peppas model:

$$\frac{M_t}{M_\infty} = kt^n \quad (1)$$

for 0-96 hours, where $\frac{M_t}{M_\infty}$ is the fraction of drug released at time *t*, *k* is the kinetic constant relating to structural characteristics, and *n* is the diffusional exponent used to describe release mechanisms.[20] Average percent dissolution across each time point for DEX HCMP and free DEX were plotted against time with standard deviations. Entrapment efficiency was found by comparing maximum dissolution from DEX-entrapped HCMPs to that of free dexamethasone.

Statistical analysis

A two-sample t-test assuming equal variances was performed on the elastic modulus measurements of 12 empty and 12 DEX-entrapped HCMPs to determine whether any significant differences (α=0.0001) in elasticity exist. The same statistical analysis was performed on cryo-SEM images to determine whether there are significant differences in particle size diameter, individual pore size, and mean gray value between 0.25 kPa and 10 kPa particles. Sample size for particle size diameter, individual pore size, and mean gray value was 38-42, 56-66, and 10 for both formulations, respectively. Results are reported as mean +/- standard deviation.

Results

HCMP ultrastructure

Cryo-SEM images revealed that the ultrastructure of soft, 0.25 kPa and stiff, 10 kPa microparticles featured non-interconnected pores (Fig. 1). Images of large, polydisperse particles made via bulk emulsion conveyed a broad view of the polymer structure, revealing a difference in pore wall thickness between soft (Fig. 1A) and stiff (Fig. 1B) particles. Session two images provided the most accurate representation of the ultrastructure of soft and stiff particles (Fig. 1C and 1D, respectively). Investigation of the microparticles' diameter using images from this session indicated that the 0.25 and 10 kPa particles did not have significantly different diameters (9.30 +/- 0.91 and 9.15 +/- 1.42 μm, respectively, $p>0.0001$) (Fig. 1G). 0.25 kPa particles exhibited individual pore size diameters that were 36% smaller than 10 kPa particles (1.47 +/- 0.51 μm vs. 2.28 +/- 0.76 μm, respectively, $p<0.0001$) (Fig. 1H). Mean gray value analysis on images from session three highlighting the differences in pore wall thickness between soft (Fig. 1E) and stiff (Fig. 1F) microparticles revealed that the 0.25 kPa particles had 33% less mean gray value area per particle, correlating to thinner polymer pore walls than 10 kPa particles (60.4 +/- 11.1 vs. 90.7 +/- 14.0, respectively, $p<0.0001$) (Fig. 1I).

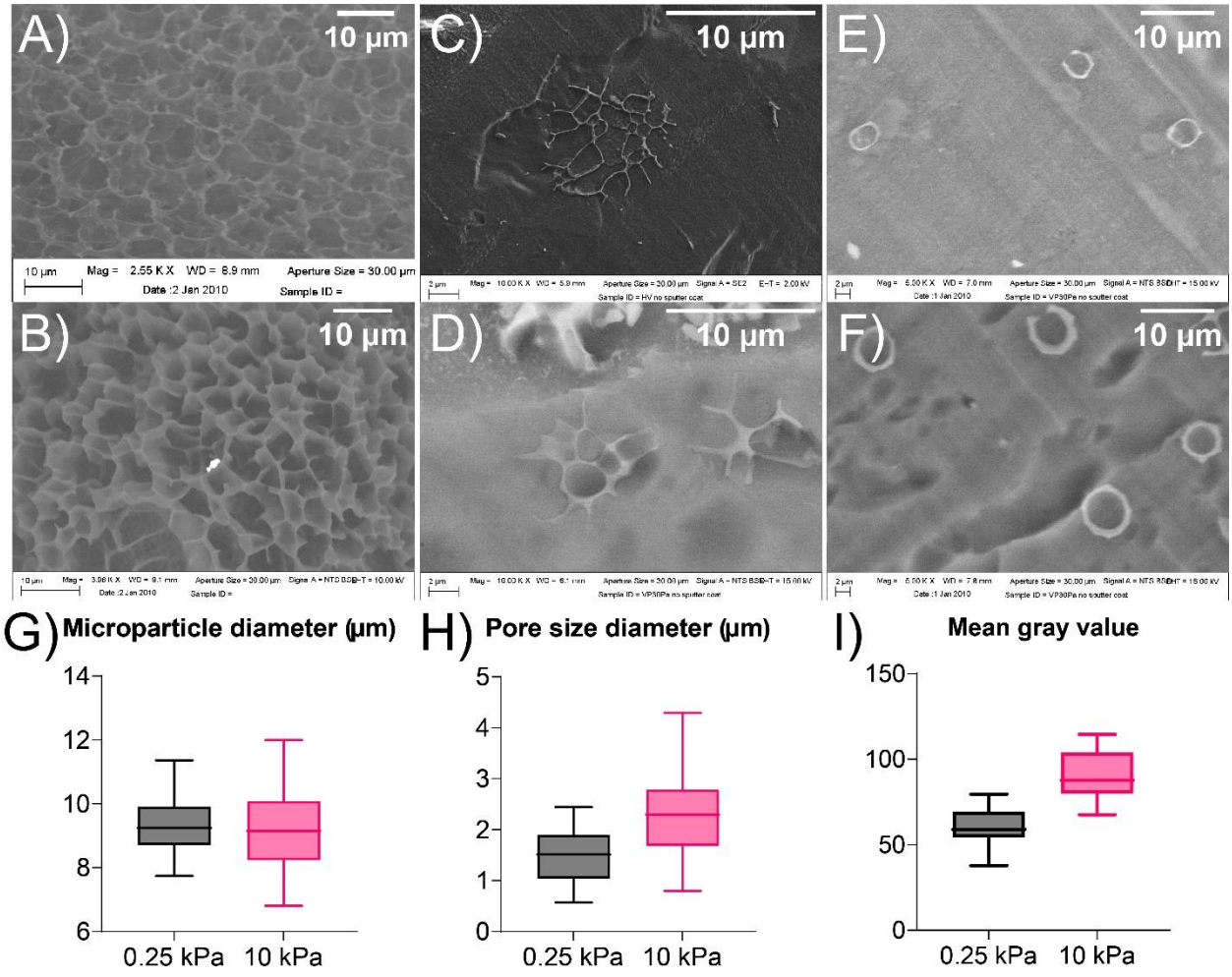

Figure 1. **Cryo-SEM on 0.25 kPa and 10 kPa microparticles:** *Soft, 0.25 kPa (A) and stiff, 10 kPa (B) large, polydisperse microparticles revealed a broad view of the porous polymer structure. Representation of the true ultrastructure of monodisperse soft (C) and stiff (D) microparticles on the internal face of a fractured droplet. Differences in polymer pore wall thickness highlighted between soft (E) and stiff (F) particles in images from session three. HCMP diameter remained similar in both particles after cryogenic preparation (G). 0.25 kPa particles possessed pore size diameters that were significantly smaller than those of 10 kPa particles (H). Significantly lower mean gray values, correlating to thinner polymer walls were exhibited in 0.25 kPa HCMPs (I). All error bars represent standard deviation.*

FITC-dextran size exclusion assay

Images revealed an exclusion of FITC-dextrans from permeating through the polymer mesh based on molecular weight (Fig. 2B and 2C). FITC alone (no attached dextran) acted as a positive control for complete permeation into microparticles, making them the same color as the

background. Image processing of the Alexa 488 channel indicated that the 0.25 kPa particles' maximum effective permeability was 22 nm, while the permeability of the 10 kPa particles was ~60% smaller, at 9 nm (Fig. 2A).

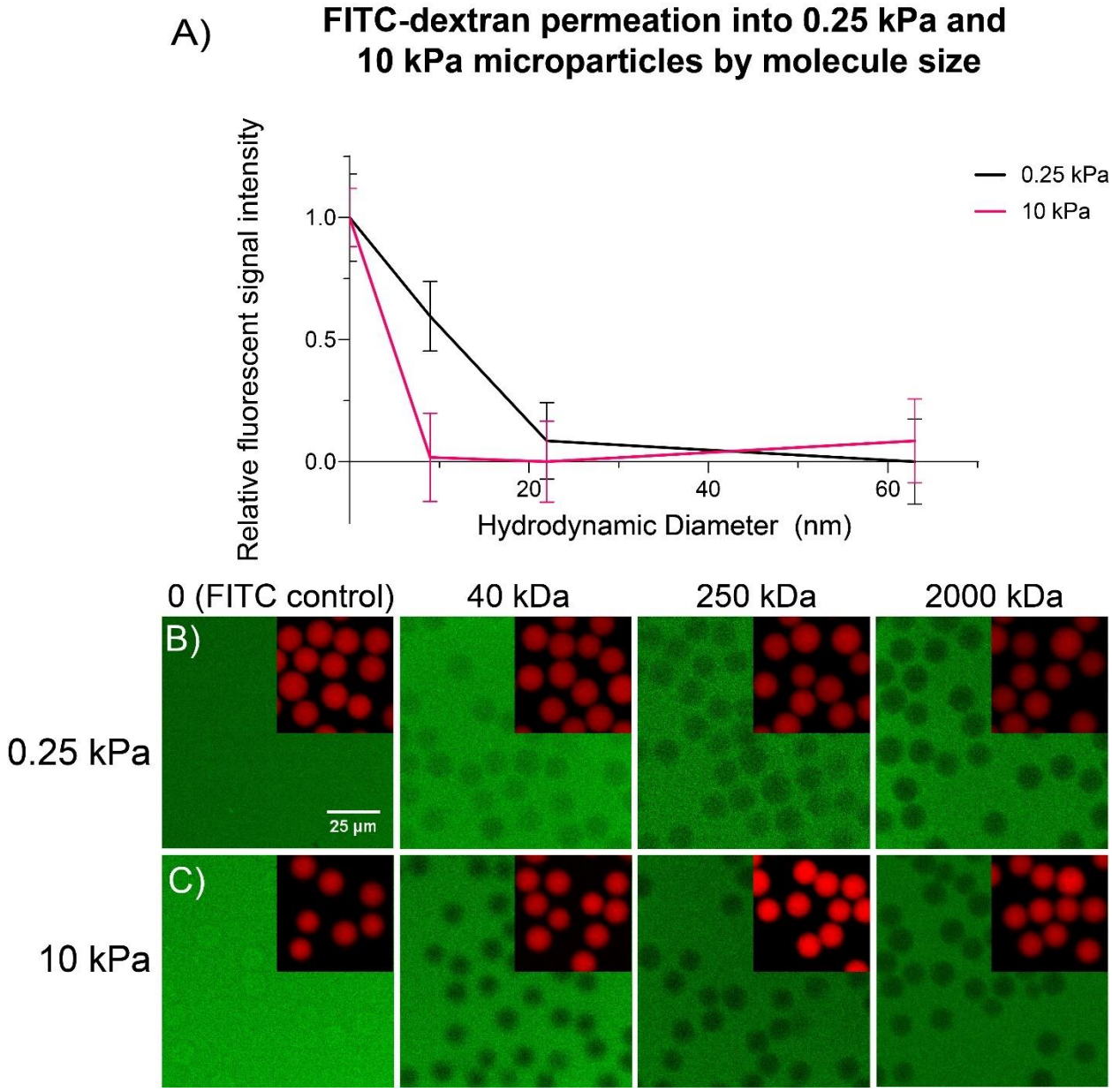

Figure 2. Size exclusion assay of HCMPs: *Analysis revealed the maximum effective permeability of 0.25 kPa microparticles was more than double that of the 10 kPa microparticles (A). Alexa 568 channel (top right) was used as a guide in the MATLAB code to locate particles in the Alexa 488 channel, which was subsequently used to analyze FITC-dextran permeation (B and C). Error bars represent standard deviation.*

Dexamethasone entrapment into HCMPs

Sonicating dexamethasone for 20 minutes broke down large aggregates (Fig. 3A) into much smaller crystals (Fig. 3B), allowing for entrapment into microparticles. Polarized light microscopy (PLM) was used after entrapment to confirm the presence of crystalline dexamethasone structure inside the amorphous polymer structure (Fig. 3C and 3D). Elasticity testing on the bulk emulsion HCMPs using the AFM revealed that there was no statistical difference in the elastic modulus of empty HCMPs and DEX-entrapped HCMPs (0.23 +/- 0.09 kPa, 0.27 +/- 0.04 kPa, respectively, p>0.0001).

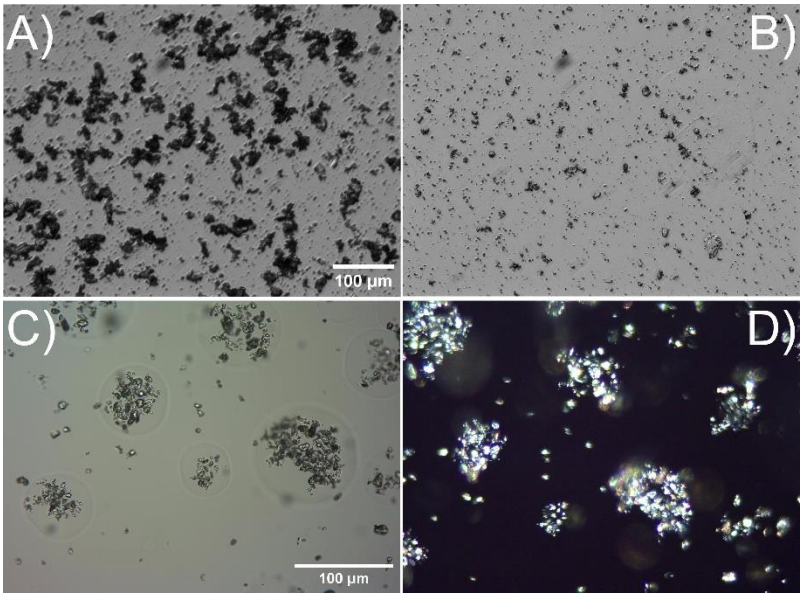

Figure 3. Sonicated DEX-entrapped HCMPs: *Images taken before (A) and after (B) sonication revealed broken down aggregates into small crystals. Brightfield microscopy (C) showed DEX-entrapped HCMPs, while PLM confirmed crystalline structure was present inside the amorphous polymer structure (D).*

Dissolution studies of entrapped vs. free dexamethasone

At 24 hours, both DEX HCMPs and free DEX had dissolved ~100% of loaded drug into the sink, but free DEX exhibited a slightly faster dissolution within this time frame (Fig. 4A). DEX HCMP and free DEX dissolution was plotted with an overlaying curve fit to the Ritger Peppas model, $\frac{M_t}{M_\infty} = kt^n$ (Eq. 1). The release profile fit the model with R^2 values ranging from 0.89-0.99.

From 0-96 hours, the DEX HCMP and free DEX fit revealed diffusional exponent describing release mechanisms, n = ~0.05 and ~0.02, while the kinetic constant relating to structural characteristics, k was 83.6 +/- 3.21, and 93.5 +/- 0.70, respectively. [20] Images of microparticles before and after dissolution revealed that all the DEX had dissolved out of the microparticles by the end of the study (Fig. 4B and 4C).

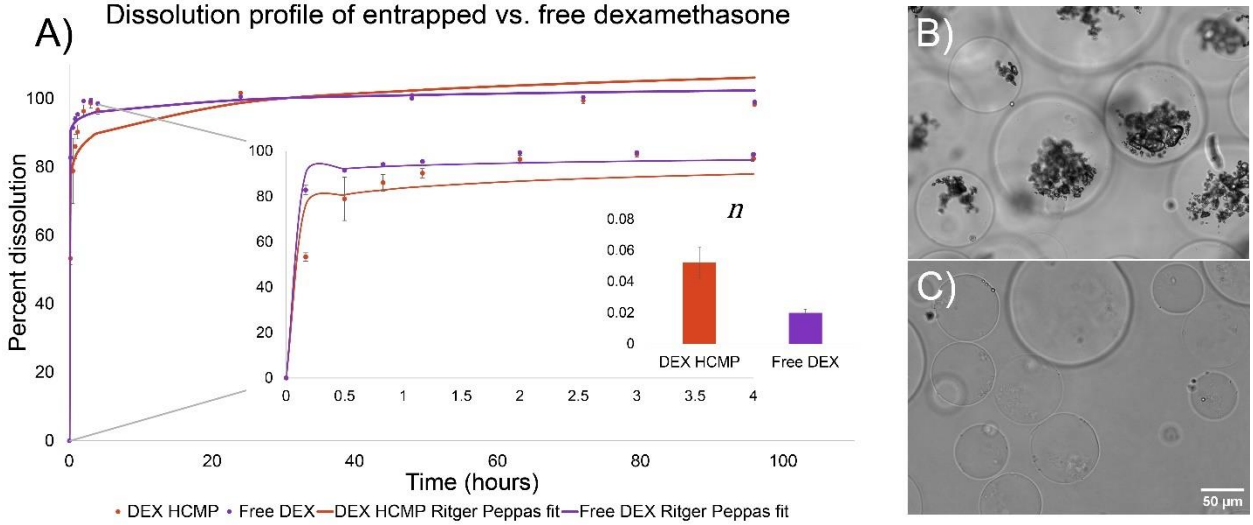

Figure 4. Dissolution profile of entrapped vs. free dexamethasone over 96 hours: *Free DEX exhibited slightly faster dissolution compared to DEX HCMPs within the first 4 hours, but both profiles had n values below 0.5 (A). Images from before (B) and after (C) dissolution revealed that all the DEX had been dissolved into the sink.*

Discussion and Conclusions

The goal of this study was to characterize the ultra and nanostructure of soft, 0.25 kPa and stiff, 10 kPa microparticles, while also entrapping dexamethasone into the soft HCMPs and comparing dissolution rates to that of free, non-entrapped drug. Results revealed that microparticles featured non-interconnected pores, with the soft HCMPs exhibiting significantly smaller pore size diameters and thinner polymer pore walls than the stiff microparticles. Maximum effective permeability was on the nanoscale for both formulations, but the permeability of the soft HCMPs was more than double that of stiff microparticles. Lastly, sonicating dexamethasone decreased the size of DEX aggregates, which allowed more even distribution inside the HCMPs. The inclusion of these small DEX crystals had no effect on the structure or stiffness of the microparticles, and the dissolution profile for free DEX was only slightly faster than entrapped DEX within the first four hours.

Cryo-SEM is an excellent method for viewing the general pore structure and polymer walls, but the harsh and inconsistent preparation techniques bring variability to the size and morphology of the samples.[21] The fracturing of the droplet and temperature consistency during imaging are both handled manually, leading to heterogeneous images obtained between each session. Session two provided the most accurate representation of the HCMP ultrastructure, as it revealed the full microparticle diameter as well as the internal pore size diameters (Fig. 1C and 1 D). These images showed a decrease in the diameter of both 0.25 kPa and 10 kPa particles from 12 to 9 μm, and because the pores are non-interconnected, we can assume that the pore size decreased to a similar proportion. It has been shown that pore size and number of pores is affected by the degree of crosslinker, with a higher concentration correlating to larger pores, and a smaller distribution.[22] Stiff particles were formulated using a higher concentration of crosslinker, resulting

in larger pores (Fig. 1H). Because microparticle diameters between the samples were not significantly different, and the 10 kPa particles had larger pore size diameters, we can also assume a fewer number of pores in the stiff particles. It is important to note at the particles from session one (Fig. 1A and 1B) cannot be analyzed for their diameter or pore size diameter because they are not monodispersed. Images from session three (Fig. 1E and 1F) also cannot be used for this analysis because only partial pore structure is visible.

Increasing crosslinker concentration increases the elastic modulus up until an inflection point, when the highly crosslinked areas can increase heterogeneity, and decrease elastic modulus.[23] After this point, the relationship between crosslinker concentration and elastic modulus becomes unclear. This point has previously been identified for polyacrylamide hydrogels consisting of 10-20% acrylamide, and 0.25-11% bis-acrylamide.[23] The acrylamide and bis-acrylamide composition used in this work was well below the reported inflection point, so we can assume a well-defined relationship. Although images from session three revealed only partial pore structure, there is a clear increase in pore wall thickness in the stiff microparticles (Fig. 1F), the same of which can be observed in the stiff polydisperse sample (Fig. 1B). We hypothesize that the thickness of these polymer pore walls is the presiding factor determining microparticle stiffness. Because the pores of these HCMPs are non-interconnected, fluid would encounter more resistance traveling from pore-to-pore as it flows through the 10 kPa microparticles, which have thicker polymer sheets, therefore increasing the effective elastic modulus.

One of the most important features of these microparticles is their non-interconnected pores, most closely resembling a honeycomb structure. There are three common types of reported hydrogel structures; honeycomb (HC), in which polymer walls are formed by non-interconnected sections parallel to each other throughout the depth of the hydrogel, fibrillar networks (FN),

consisting of completely interconnected pores, and broken interconnected films (BIF), which are partially connected by filaments.[24] Because the FN and BIF pore structure feature either partial or full connection from pore-to-pore, the HCMPs fabricated in this study most closely identify with the HC structure, best seen in Fig. 1A and 1B. This feature is important for entrapment and dissolution because drug release into the surrounding environment depends on its diffusion through the polymer mesh. This indicates that the minimum size of DEX nanocrystals required for entrapment is defined by the effective permeability of the polymer mesh. Microparticles with higher crosslinking densities, such as the stiff HCMPs will exhibit a decrease in effective permeability, or in turn, an increase the size selectivity.[25] DEX nanocrystals would need to be 22 nm or above to remain entrapped in the monodisperse soft HCMPs because the mesh excluded the 250 kDa (22 nm) FITC-dextrans (Fig. 2A). This is more than double the effective permeability of the stiff particles, meaning the nanocrystals would need to be larger to remain entrapped in the softer particles. Any crystals smaller than this size would likely be lost during the washing process, decreasing encapsulation efficiency. It should be noted that the dextran used in this study may have some heterogeneity in size, so what appears as fractional permeation of 40 kDa FITC-dextran into 0.25 kPa microparticles, was considered to be full permeation when interpreting the data. Most likely, the actual effective permeability of the polymer mesh lies between 9 and 22 nm, which reflects the resolution limit of the dextran molecular weights used in the experiment.

Effective permeability of the polymer mesh, as well as the drug's physical and chemical characteristics are some of the properties determining the rate of release. An increase in permeability, as seen in the soft microparticles may contribute to an increase in the drug release rate by dissolution.[26] Although the dexamethasone was sonicated, we still see proof of some aggregation in microparticles due to hydrophobicity of the drug (Fig. 3D). Even so, the aggregates

within the microparticles may still be smaller than those in the free DEX sink because they can only be as large as the size of the pore in which they are entrapped. The amount of aggregation will affect the surface area to volume ratio, which directly correlates to the drug release rate.[27] This ratio is described in equation 2:

$$\frac{M_t}{M_\infty} = 2\left(\frac{SA}{Vol}\right)\left(\frac{D_{eff}t}{\pi}\right)^{\frac{1}{2}} \quad (2)$$

where $\frac{M_t}{M_\infty}$ is the release rate, *SA* is the drug surface area, *Vol* is the drug volume, and D_{eff} is the drug diffusion coefficient.[27] As dexamethasone aggregates become larger in the microparticles or at the bottom of the sink, the surface area to volume ratio decreases, slowing down the dissolution rate. Therefore, the dissolution rate may be adjusted by tuning the size of the entrapped drug crystal.

Drug release is typically defined by polymer erosion, diffusion through a swollen matrix, or release from the surface of the particles.[20] Most often, however, drug release is governed by more than one of these mechanisms.[20] Ritger Peppas (Eq. 1) is a popular kinetic model that has often been used to describe drug release through Fickian and anomalous diffusion. This model, $\frac{M_t}{M_\infty} = kt^n$ indicates that when $n = 0.5$, the process is Fickian diffusion, $0.5 < n < 1$ represents anomalous non-Fickian solute diffusion, and $n = 1$ is zero order case II transport.[28] However, these values are dependent on the nature of the polymer and study. For example, in polydisperse samples, these values change to $n = 0.43$ instead of 0.5, and 0.85 instead of 1.[20] The *n* value for DEX HCMP and free DEX dissolution are both below 0.43, suggesting quasi-Fickian diffusion through the swollen polyacrylamide matrix of the HCMPs.[28] The rate of diffusion is largely affected by the chemical structure of the hydrogel, specifically the swelling ratio.[28] Hydrogels possessing higher initial swelling ratios will quickly release the drug, as the pores immediately fill with water.[28]

Because the soft microparticles used in this study were made of > 99% water, Q will be very high, contributing to the quick release observed.

Kinetic constant, k in Eq.1 which was higher for free DEX than DEX-entrapped HCMPs, depends largely on the geometric and structural characteristics of the system.[20] The higher kinetics in free DEX is observed mainly in the first four hours before both curves reach a plateau (Fig 4A). We hypothesize that this very slight delay in release from the HCMPs occurs because the drug needs to pass through the polymer sheets making up the pore walls and the microparticle surface. This, in combination with the potential presence of a temporary "cloud" of higher concentration of DEX in the HCMP pores diminishes the concentration gradient from one pore to the next. As soon as the DEX diffuses through this gradient, it should release into the sink at the same rate as the free DEX. While it is important to acknowledge that the free DEX dissolution does slightly differ from the entrapped DEX, the discrepancies are so minor that they may be considered negligible in the full dissolution profile. In addition, if the difference is indeed due to a temporary concentration of DEX in the outer ring of internal pores, this would be cleared *in-vivo* due to continuous flow of the microparticles.

This work is the first to demonstrate release characteristics of dexamethasone nanocrystals from an extremely soft, cell-like carrier. However, it should be noted that the microparticles were fabricated in a bulk-emulsion, leading to large, polydisperse samples not viable for *in-vivo* delivery. Future steps include making smaller, 10 μm monodisperse particles, which can be fabricated with droplet generation like the those used in cryo-SEM and the size exclusion assay. To entrap a drug like DEX into 10 μm particles, it would need to be broken up into even smaller crystals to avoid disrupting the elastic modulus or structure. This may be achieved by sonicating more extensively and filtering any crystals larger than 1-2 μm in diameter before loading into the

microparticles. More repetitions of cryo-SEM on soft and stiff particles should also be performed to gain a better understanding of how the ultrastructure influences elastic modulus.

Although all of the drug was released in the first 24 hours, these microparticles still have potential therapeutic use for long-term, sustained drug release. Because we know that entrapping a nano-sized substrate would not disrupt the structure or elasticity of these microparticles, future studies should focus on entrapping the drug into biodegradable polymer nanoparticles for controlled, long-term release, and then entrapping the nanoparticles themselves into HCMPs. We also observed no hindrance in release of DEX from the microparticles, meaning the drug release would only be controlled by the nanoparticle's mechanism. The HCMPs would act more as a carrier to avoid phagocytosis, as they mimic the shape, size, and elasticity of living mammalian cells.

References

1. Herman, T. F., & Santos, C. (2022). First Pass Effect. In *StatPearls*. StatPearls Publishing.
2. Bolger, G. T. (2018). Routes of Drug Administration. *Reference Module in Biomedical Sciences*. https://doi.org/10.1016/b978-0-12-801238-3.11099-2
3. Singh, M. N., Hemant, K. S., Ram, M., & Shivakumar, H. G. (2010). Microencapsulation: A promising technique for controlled drug delivery. *Research in pharmaceutical sciences*, *5*(2), 65–77.
4. Lengyel, M., Kállai-Szabó, N., Antal, V., Laki, A. J., & Antal, I. (2019). Microparticles, microspheres, and microcapsules for Advanced Drug Delivery. *Scientia Pharmaceutica*, *87*(3), 20. https://doi.org/10.3390/scipharm87030020
5. Brannon, E. R., Guevara, M. V., Pacifici, N. J., Lee, J. K., Lewis, J. S., & Eniola-Adefeso, O. (2022). Polymeric particle-based therapies for acute inflammatory diseases. *Nature Reviews Materials*, *7*(10), 796–813. https://doi.org/10.1038/s41578-022-00458-5
6. Cooley, M., Sarode, A., Hoore, M., Fedosov, D. A., Mitragotri, S., & Sen Gupta, A. (2018). Influence of particle size and shape on their margination and wall-adhesion: Implications in drug delivery vehicle design across nano-to-micro scale. *Nanoscale*, *10*(32), 15350–15364. https://doi.org/10.1039/c8nr04042g
7. Suk, J. S., Xu, Q., Kim, N., Hanes, J., & Ensign, L. M. (2016). Pegylation as a strategy for improving nanoparticle-based drug and Gene Delivery. *Advanced Drug Delivery Reviews*, *99*, 28–51. https://doi.org/10.1016/j.addr.2015.09.012
8. Merkel, T. J., Jones, S. W., Herilhy, K. P., Kersey, F. R., Shields, A. R., Napier, M., Luft, J. C., Wu, H., Zamboni, W. C., Wang, A. Z., Bear, J. E., & DeSimone, J. M. (2011). Using mechanobiological mimicry of red blood cells to extend circulation times of hydrogel microparticles. *PNAS*, 108 (2) 586-591. https://www.pnas.org/doi/pdf/10.1073/pnas.1010013108
9. Tan, M. L., Choong, P. F. M., & Dass, C. R. (2010). Recent developments in liposomes, microparticles and nanoparticles for protein and peptide drug delivery. *Peptides*, *31*(1), 184–193. https://doi.org/10.1016/j.peptides.2009.10.002
10. Kim, D.-H., & Martin, D. C. (2006). Sustained release of dexamethasone from hydrophilic matrices using PLGA nanoparticles for neural drug delivery. *Biomaterials*, *27*(15), 3031–3037. https://doi.org/10.1016/j.biomaterials.2005.12.021
11. Anselmo, A. C., Zhang, M., Kumar, S., Vogus, D. R., Menegatti, S., Helgeson, M. E., & Mitragotri, S. (2015). Elasticity of nanoparticles influences their blood circulation, phagocytosis, endocytosis, and targeting. *ACS Nano*, *9*(3), 3169–3177. https://doi.org/10.1021/acsnano.5b00147
12. Tang, F., Chen, D., Zhang, S., Hu, W., Chen, J., Zhou, H., Zeng, Z., & Wang, X. (2020). Elastic hysteresis loop acts as cell deformability in erythrocyte aging. *Biochimica Et Biophysica Acta (BBA) - Biomembranes*, *1862*(7), 183309. https://doi.org/10.1016/j.bbamem.2020.183309

13. Labriola, N. R., Mathiowitz, E., & Darling, E. M. (2017). Fabricating polyacrylamide microbeads by inverse emulsification to mimic the size and elasticity of living cells. *Biomaterials Science*, *5*(1), 41–45. https://doi.org/10.1039/c6bm00692b
14. Franco, F., Pérez-Maqueda, L. A., & Pérez-Rodríguez J.L. (2004). The effect of ultrasound on the particle size and structural disorder of a well-ordered kaolinite. *Journal of Colloid and Interface Science*, *274*(1), 107–117. https://doi.org/10.1016/j.jcis.2003.12.003
15. Pluronic™ F-127 (20% solution in DMSO). *Thermo Fisher Scientific*, https://www.thermofisher.com/order/catalog/product/P3000MP#:~:text=Pluronic%20F%2D127%20*20%25,other%20materials%20in%20physiological%20media
16. Dubay, R., Fiering, J., & Darling, E. M. (2020). Effect of elastic modulus on inertial displacement of cell-like particles in Microchannels. *Biomicrofluidics, 14*(4), 044110. https://doi.org/10.1063/5.0017770
17. Liu, J., Teng, P.-Y., Kim, W. K., & Applegate, T. J. (2021). Assay considerations for fluorescein isothiocyanate-dextran (FITC-D): An indicator of intestinal permeability in broiler chickens. *Poultry Science, 100*(7), 101202. https://doi.org/10.1016/j.psj.2021.101202
18. Fluorescein isothiocyanate-dextran. *Millipore Sigma*, https://www.sigmaaldrich.com/US/en/technical-documents/technical-article/cell-culture-and-cell-culture-analysis/cell-based-assays/fluorescein-isothiocyanate-dextran
19. Dexamethasone. *PubChem*, https://pubchem.ncbi.nlm.nih.gov/compound/Dexamethasone
20. Unagolla, J. M., & Jayasuriya, A. C. (2018). Drug transport mechanisms and in vitro release kinetics of vancomycin encapsulated chitosan-alginate polyelectrolyte microparticles as a controlled drug delivery system. *European journal of pharmaceutical sciences : official journal of the European Federation for Pharmaceutical Sciences*, *114*, 199–209. https://doi.org/10.1016/j.ejps.2017.12.012
21. Aston, R., Sewell, K., Klein, T., Lawrie, G., & Grøndahl, L. (2016). Evaluation of the impact of freezing preparation techniques on the characterisation of alginate hydrogels by cryo-SEM. *European Polymer Journal*, *82*, 1–15. https://doi.org/10.1016/j.eurpolymj.2016.06.025
22. Mirzaei B., E., Ramazani S. A., A., Shafiee, M., & Danaei, M. (2013). Studies on glutaraldehyde crosslinked chitosan hydrogel properties for Drug Delivery Systems. *International Journal of Polymeric Materials*, *62*(11), 605–611. https://doi.org/10.1080/00914037.2013.769165
23. Denisin, A. K., & Pruitt, B. L. (2016). Tuning the range of polyacrylamide gel stiffness for mechanobiology applications. *ACS Applied Materials & Interfaces, 8*(34), 21893–21902. https://doi.org/10.1021/acsami.5b09344
24. Pacios, I.E., Pastoriza, A. & Pierola, I.F. Effect of the crosslinking density and the method of sample preparation on the observed microstructure of macroporous and conventional poly(*N*,*N*-dimethylacrylamide) hydrogels. *Colloid Polym Sci* **285**, 263–272 (2006). https://doi.org/10.1007/s00396-006-1559-7

25. Dai, W. S., & Barbari, T. A. (1999). Hydrogel membranes with mesh size asymmetry based on the gradient crosslinking of poly(vinyl alcohol). *Journal of Membrane Science*, *156*(1), 67–79. https://doi.org/10.1016/s0376-7388(98)00330-5
26. Chavda, H., & Patel, C. (2011). Effect of crosslinker concentration on characteristics of superporous hydrogel. *International journal of pharmaceutical investigation*, *1*(1), 17–21. https://doi.org/10.4103/2230-973X.76724
27. Reynolds, T. D., Mitchell, S. A., & Balwinski, K. M. (2002). Investigation of the effect of tablet surface area/volume on drug release from hydroxypropylmethylcellulose controlled-release matrix tablets. *Drug Development and Industrial Pharmacy*, *28*(4), 457–466. https://doi.org/10.1081/ddc-120003007
28. Jamnongkan, T., & Kaewpirom, S. (2010). Potassium release kinetics and water retention of controlled-release fertilizers based on Chitosan Hydrogels. *Journal of Polymers and the Environment*, *18*(3), 413–421. https://doi.org/10.1007/s10924-010-0228-6